Am J Cancer Res 2026;16(8):3338-3358
www.ajcr.us /ISSN:2156-6976/ajcr0173630

Original Article

Dual role of HIF-1α in gliomas: enhancing COX7A2 degradation and SCAF1 expression for ATP production and tumor progression

Minfang Lai[2], Wenping Feng[1], Jinyou Ouyang[1], Jianguo Kuang[1], Shengze Deng[1]

[1]Department of Neurosurgery, The First Affiliated Hospital, Jiangxi Medical College, Nanchang University, Nanchang 330006, Jiangxi, China; [2]Department of Pharmacy, The First Affiliated Hospital, Jiangxi Medical College, Nanchang University, Nanchang 330006, Jiangxi, China

Received April 27, 2026; Accepted June 28, 2026; Epub August 15, 2026; Published August 30, 2026

Abstract: Objective: To investigate whether HIF-1α promotes SCAF1/COX7A2 replacement in complex IV and thereby influences glioma progression. Methods: A172 and U251 cells were subjected to $CoCl_2$-induced hypoxia. The effects of hypoxia on cell behavior were assessed via CCK-8 for viability and Transwell for migration and invasion. Stable cell lines overexpressing HIF-1α, SCAF1, or CLPP, or knocking down COX7A2, LONP1, or CLPP were established. Mitochondrial supercomplex composition was analyzed by Blue Native PAGE. HIF-1α's binding to the SCAF1 promoter was validated by ChIP and dual-luciferase assays. Protein interactions were examined by Co-IP and GST pull-down. Xenograft tumor growth experiments conducted in nude mice was evaluated following COX7A2 overexpression or SCAF1 knockdown in tumor growth. Results: $CoCl_2$ treatment significantly increased cell viability, migration, invasion, ATP concentration and the formation of I+III_2+IV of glioma cells, and similar effects were observed upon HIF-1α overexpression, COX7A2 knockdown, or SCAF1 overexpression. HIF-1α targeted the SCAF1 promoter to regulate its expression, and HIF-1α regulated COX7A2 protein levels through LONP1 and CLPP. In the tumorigenesis experiment in nude mice, SCAF1 knockdown reduced tumor volume and weight, while COX7A2 overexpression reduced tumor volume and weight. Conclusion: Hypoxia in glioma cells enhances cell viability, migration, invasion, ATP production, and I+III_2+IV supercomplex formation, with HIF-1α regulating SCAF1 and COX7A2 levels. These findings highlight the promising potential of targeting the HIF-1α/SCAF1/COX7A2 pathway as a treatment option for glioma treatment.

Keywords: Hypoxia, glioma, oxidative phosphorylation, COX7A2, SCAF1, ATP production

Introduction

Gliomas is a common form of high-grade brain tumor [1, 2]. The standard treatment for Glioma patients involves a chemotherapy regimen of temozolomide [3]. However, the complex biology of Gliomas makes effective treatment challenging, resulting in poor clinical prognosis, with a median survival of only 14.6 months [4]. There is an urgent need to unravel the molecular mechanisms involved in glioma development to identify novel drug targets.

Most of the chemical energy (ATP) available to cells and tissues meet their energy demands primarily through oxidative phosphorylation (OXPHOS). It is the synergistic action of five polymeric enzyme complexes (CI-CV), embedded in the lipid bilayers of the inner mitochondrial membrane, that constitutes this system [5]. The term "mitochondrial respiratory chain (MRC)" refers specifically to the first four enzyme complexes (CI-CIV), through which electrons reduce O_2 to water [6]. What constitutes the terminal enzyme of the mitochondrial respiratory chain is cytochrome c oxidase (CcO, Complex IV), consisting of 14 subunits [7-9]. COX7A is one of the subunits with tissue- and species-specific subtypes [6]. Cox7A1 is tissue-specifically expressed in the skeletal muscle in conjunction with cardiac muscle, while Cox7A2 is a liver-type subtype and is commonly expressed [10, 11]. Previous studies have shown the clinical prognosis correlates with the COX7A2 expression in Barrett's adenocarcinoma [12]. Cox7A2 is also strongly associated

https://doi.org/10.62347/RIKY8807

with ovarian cancer patients' prognosis [13]. In our earlier research, we demonstrated that glioma patients with high COX7A2 expression have a good prognosis, and COX7A2 can be used as an independent prognostic factor [14]. However, what function COX7A2 exerts in glioma pathogenesis remains to be determined.

The larger supramolecular structures in the mitochondrial respiratory chain, including supercomplexes (SCs), respirasomes and giant complexes, are composed of complexes I, III and IV (CI, $CIII_2$ and CIV) [15-17]. To adapt to the increased energy demand of cells and improve the operational efficiency of the mitochondrial respiratory chain, supercomplexes (SCs) may be formed [18, 19]. Supercomplex assembly factor 1 (SCAF1) is molecularly similar to COX7A2, also known as COX7A2L or COX7RP. Both SCAF1 and COX7A2 can be interchangeable, resulting in a change in the assembly form of Complex IV. Studies have shown that the CIV subunit COX7A2 is not present in CIII-CIV supercomplexes, being replaced instead by SCAF1 [20]. Therefore, in gliomas, which mechanism induces SCAF1 to replace COX7A2?

Studies have shown that COX7A2L is induced to express in situations of cellular stress, including hypoxia, ER stress, and nutritional stress, promoting the formation of mammalian cells SC [21-23]. It is the extensive hypoxia and necrosis in glioblastomas that make the role of hypoxia in driving tumor growth increasingly important [21, 24]. Therefore, hypoxia may induce SCAF1 to replace COX7A2 in gliomas. Transcriptional adaptation to hypoxia is mainly regulated by hypoxia-inducing factors (HIF), including HIFα (1-3), aromatic receptor nuclear transporter (ARNT) and ARNT2 [22, 23, 25]. Under normal oxygen tension conditions, HIF1α, HIF2α, and HIF3α in the cytoplasm are rapidly degraded by the ubiquitin pathway [23]. In hypoxic conditions, HIF stabilizes and translocates to the nucleus, forming a dimer with ARNT or ARNT2. These heterodimers bind genomic DNA at sites called hypoxic response elements (HRE) to regulate transcription [23]. In this study, six candidate HREs for the promoter of SCAF1 were predicted through the JASPAR database, indicating that SCAF1 is also the target gene of HIF-1α. Therefore, we hypothesize that HIF-1 might mediate the conversion of SCAF1 and COX7A2 when assembling the mitochondrial respiratory chain complex IV into a supercomplex by regulating SCAF1 expression, thereby altering the activity of the mitochondrial respiratory chain and affecting the production of ATP in cells.

In addition to upregulating SCAF1 expression to increase the probability of SCAF1 and COX7A2 exchange, does HIF-1α affect COX7A2 expression and what is the mechanism? Our previous study found that the COX7A2 gene is activated without HREs, so HIF-1α may regulate the level of COX7A2 by influencing other proteins. Mitochondrial protease LON (LONP1) is highly conserved during evolution and is an ATP-dependent protease. Studies have shown that LONP1 gene transcription is activated by HIF-1, leading to the modulation of COX4 subunit expression [26]. However, further research is needed to determine if HIF-1α can also degrade COX7A2 by influencing the level of LONP1.

LONP1 and CLPP share many substrates, which can work synergistically to reduce protein toxic stress and protect mitochondrial function to promote prostate cancer cell survival [27]. It is the reduction in the ATP-dependent activity of LONP1 and/or CLPP under hypoxia that causes mitochondrial transcripts to aggregate [28]. Therefore, it is important to explore whether CLPP also plays a significant role in HIF-1α-mediated degradation of COX7A2.

Therefore, we hypothesized that HIF-1α may enhance the degradation of COX7A2 by regulating LONP1 and CLPP, while also upregulating SCAF1 expression. This dual mechanism could facilitate the replacement of COX7A2 with SCAF1, leading to increased ATP production and the advancement of glioma progression.

Materials and methods

Cell lines culture and chemical hypoxia

Human glioma cell lines A172 (CL-0012) and U251 (CL-0237), obtained from Wuhan Pricella Biotechnology Co., Ltd., were used for *in vitro* experiments. After thawing, cells were resuspended in DMEM medium (VivaCell, C3113-0500). DMEM was supplemented with 10% (v/v) FBS (BI, 04-001-1ACS) and 1% (v/v) P/S (GENOM Bio, GNM15140) to prepare the com-

Table 1. List of RNA interference sequences used in this study

Gene	Sequence (5'→3')
sh-COX7A2	
sh-COX7A2-1	GATCCTGTATAGAGCCACCATGATTCTCGAGAATCATGGTGGCTCTATACAGTTTTTG
sh-COX7A2-2	GATCCCGATTCCACAGTGTATGATTCTCGAGAATCATACACTGTGGAATCGGTTTTTG
sh-COX7A2-3	GATCCCTGCCTGACCAAATGCTTTACTCGAGTAAAGCATTTGGTCAGGCAGGTTTTTG
si-LONP1	
si-LONP1-1	S: GAGAAGGUGUUACGGAAAUTT
	A: AUUUCCGUAACACCUUCUCTT
si-LONP1-2	S: GUCGGCGUCUUUCUAAAGATT
	A: UCUUUAGAAAGACGCCGACTT
si-LONP1-3	S: GGGACAUCAUUGCCUUGAATT
	A: UUCAAGGCAAUGAUGUCCCTT
si-CLPP	
sh-CLPP-1	S: CCCGAUCGAUGACAGCGUUTT
	A: AACGCUGUCAUCGAUCGGGTT
sh-CLPP-2	S: GAGAUCAUGAAGCUCAAGATT
	A: UCUUGAGCUUCAUGAUCUCTT
sh-CLPP-3	S: CCAGGAGUUUGGCAUCUUATT
	A: UAAGAUGCCAAACUCCUGGTT
siNC	
siNC	S: UUCUCCGAACGUGUCACGUTT
	A: ACGUGACACGUUCGGAGAATT

plete growth medium. As previously described [29], $CoCl_2$ (Sigma, 232696), an inducer of HIF-1, was used. After being seeded in 12-well plates at 1 × 10^5 cells/well, A172 and U251 cells were exposed to final concentrations of 150 μM $CoCl_2$ for 6, 24, or 72 h.

Lentivirus-mediated stable transduction and siRNA transfection

The lentiviruses were provided by Shanghai JUSTSCIENCE Co., Ltd. (China). Using restriction enzyme digestion and ligation techniques, the CDS regions of HIF-1α, SCAF1, and CLPP were respectively cloned into the JS037 vector (EcoR I → Xho I) to construct overexpression recombinant plasmids; additionally, shRNA sequences targeting COX7A2 were inserted into the JS039 vector (BamH I → EcoR I) to construct sh-COX7A2-1/2/3. After amplification, the plasmids were mixed with psPAX2 and pMD2.G plasmids along with a transfection reagent, in serum-free Opti-MEM (Gibco, 31985070). The transfection mixture was then added to 293T cells and incubated for 4 h before replacing with complete medium for further cultivation. After 48-72 h, after collection, the supernatant was filtered through a 0.45 μm filter. Cells were prepared as a suspension at 5 × 10^4 cells/mL in complete medium and subsequently transduced with the virus based on MOI along with Polybrene (Solarbio, H8761). Positive cells were selected using Puromycin (Shanghai Shaoxin Biotechnology Co., Ltd., SX50113).

The si-LONP1 and si-CLPP sequences were synthesized by GenePharm (Shanghai, China). Transfection was carried out when cells seeded in 24-well plates reached 50-70% confluence. siRNA and GP-transfect-Mate were processed for dilution in Opti-MEM, 5 min in advance, and then mixed for 20 min. Whereafter, cell samples were exposed to the formulated transfection mixture and kept at 37°C for 6 h before replacing with complete medium for further cultivation.

The transfection efficiency was assessed using RT-qPCR and Western blotting. Sequences for shCOX7A, siLONP1, and si-CLPP were listed in **Table 1**.

CCK-8 assay

Changes in cell viability were examined using the CCK-8 detection method (Beyotime, C0039). After subjecting cells to hypoxia treatment (150 μM $CoCl_2$) or lentiviral infection, CCK-8 reagent was supplemented into the cell cultures at 0, 24, 48, and 72 h, and kept for an additional hour in a 37°C. A microplate reader (Thermo, Model 1510) was used to record absorbance at 450 nm.

Transwell assay

Membrane inserts characterized by 8 μm porous structure (Corning) are designed to quantify the migratory and invasive ability of target cells. At the start of the migration test, cells were placed in the top chamber of Transwells pre-filled with serum-free medium, and a complete medium was filled in the bottom chambers. Different from the migration assay, the invasion assay required the Transwell inserts to be pre-coated with Orgmatrix gel (GENOM Bio, 111005). Specifically, the orgmatrix gel was diluted with pre-chilled (4°C) serum-free medium to a final concentration of 0.5 mg/ml before coating. Dispense 60 μL of the diluted solution evenly onto the surface of the upper chamber membrane of the Transwell chamber, then place the coated chamber in a 37°C, 5% CO_2 incubator and leave to stand for 1 hour. Cells and culture medium were then added in the same way. The plates were placed in a 37°C incubator and incubated for 24 h. Fixed and stained with 0.05% crystal violet were the migrated and invaded cells (Beyotime, C0121) for 30 min, and images of the stained cells were acquired with the aid of an Olympus light microscope.

ATP assay

Using an ATP assay kit (Beyotime, S0026), we evaluated ATP levels in cells or cancer tissues. To measure ATP, we collected the cells, lysed them, and obtained the supernatant. For cancer tissues, samples were first homogenized before lysis. The ATP assay solution and test samples were added sequentially, with at least 2 s reaction to ensure accurate measurements, followed by detection of relative luminescence units (RLU) using a microplate reader.

Blue native polyacrylamide gel electrophoresis (BN-PAGE)

BN-PAGE [30], a technique used to separate membrane protein complexes and assemblies, was employed in this study to detect the composition or activity of mitochondrial respiratory supercomplexes. Approximately 5×10^7 cells that underwent hypoxic treatment (150 μM $CoCl_2$) or lentivirus infection, or cancer tissues, were collected, lysed in pre-chilled Lysis Buffer, and homogenized with ice-cold grinding. Repeated centrifugation steps ensured effective separation of mitochondria from other cellular components. High-purity mitochondria were then resuspended in PBS loading a protease inhibitor cocktail, and we assessed the protein concentration by the bicinchoninic acid method (Beyotime, P0009). Digitonin (at a 1:8 ratio; MCE, HY-N4000) was pipetted into the mitochondrial suspension, and the sample was kept on ice. Mitochondrial protein was loaded onto a pre-prepared non-denaturing GLASS Gel Hepes-Tris gel (Shanghai Shenger Biotechnology Co., LTD., SKV-0052). After loading the samples, electrophoresis was performed at 4°C, initially at 70 V for 30 minutes, then at 150 V for 2-3 h until the dye front reached the bottom of the gel, after which Western blotting was carried out.

Assessment of mitochondrial oxygen consumption and extracellular acidification

The Elabscience Oxygen Consumption Rate (OCR) and Extracellular Acidification Rate (ECAR) Fluorescence Assay Kits were used to measure OCR and ECAR in the cells, respectively. All procedures were carried out in strict accordance with the kit instructions. A graph plotting fluorescence intensity against time was plotted, and the slope was determined from the time interval where the fluorescence intensity showed a linear relationship with time; this slope was then used to indicate the changes in OCR and ECAR.

Flow cytometry

Mitochondrial membrane potential (ΔΨm) was measured using the JC-1 Mitochondrial Membrane Potential Assay Kit (Tongren Chemical). U251 cells from each group were treated with trypsin, washed with PBS, and

Table 2. List of primer sequences for RT-qPCR analysis of target genes

Target Gene	Sequence (5'→3')
H-HIF-1α-F	GCCAGACGATCATGCAGCTA
H-HIF-1α-R	GCAGTCTACATGCTAAATCAGAGG
H-COX7A2-F	TTGGGCAGAGGACGATAAGC
H-COX7A2-R	TGGCTCTATACAGGAGGGCA
H-SCAF1-F	GACACGGCTACTGTGTTGGA
H-SCAF1-R	GCTCCAGCATGTCCTCACTT
H-LONP-F	GGTCATAACGGCGCTCACG
H-LONP-R	TCTCGACCACATCCGACTCA
H-CLPP-F	GTGGAGCAGACGGGTC
H-CLPP-R	GGCTTCTTGTTGCTCTCGGA
H-GAPDH-F	GTTCGTCATGGGTGTGAACC
H-GAPDH-R	CATCCACAGTCTTCTGGGTG

then incubated with JC-1 staining solution at 37°C in the dark for 15 minutes. Following staining, the cells were centrifuged, washed, resuspended in buffer, and immediately analyzed by flow cytometry. Mitochondrial membrane potential was detected via the FL1 channel (green fluorescence) and the FL2 channel (red fluorescence), with results expressed as the ratio of red to green fluorescence intensities.

Western blotting

Protein levels of SCAF1 (1:1000; Affinity, AF9193, 139 kDa), COX7A2 (1:1000; Affinity, AF9048, 12 kDa), HIF-1α (1:1000; Affinity, BF8002, 120 kDa), LONP1 (1:1000; Affinity, DF12119, 100 kDa), and CLPP (1:1000; Proteintech, 6271-1-Ig, 30 kDa) were detected by Western blot analysis. Protein samples or mitochondrial protein samples extracted from pre-cooled cell lysis buffer were denatured and we electrophoresed the samples on a 10% SDS-polyacrylamide gel, followed by transfer to a nitrocellulose membrane (Pall, 66485). We incubated the membrane with a blocking solution of 5% nonfat dry milk (Sangon, A600669-0250) for 1 h. Primary antibody probing took place overnight at 4°C, with antibodies used at the dilutions indicated. The membrane was used with the corresponding secondary antibodies at room temperature. An ultra-sensitive ECL solution (Beyotime, P0018S) was used to visualize the peroxidase-conjugated bands, which were then captured using the Tanon 4600 system (Tanon Science and Technology Co., Ltd.). GAPDH (1:5000; Abways, AB0036, 36 kDa) served as normalization of target proteins.

In this study, GAPDH was used as an internal loading control. Given that GAPDH is a glycolytic enzyme, it may be transcriptionally up-regulated by HIF-1α under hypoxic conditions. However, previous studies have shown that GAPDH expression is not regulated by hypoxia in the human glioblastoma cell lines U373, U251 and GaMG, and that GAPDH is an ideal loading control for determining the expression of hypoxia-induced genes in glioblastoma [31]. Furthermore, no regulation of GAPDH expression by hypoxia was observed in hepatocellular carcinoma, lung adenocarcinoma and colorectal cancer cells [32]. Consistent with these reports, we carefully examined the GAPDH band intensities under all conditions in our Western blot analyses and found them to be highly consistent. Therefore, GAPDH is considered a reliable internal loading control in the hypoxia experiments of this study.

Reverse transcription-quantitative PCR (RT-qPCR)

mRNA abundance of HIF-1α, COX7A2, SCAF1, LONP1, and CLPP in cells was assessed using real-time RT-PCR. The primer sequences are listed in **Table 2**. Cells were processed using TRIzol™ reagent (Invitrogen, 15596026), and total RNA was purified using the Tri Reagent method. RNA concentration was measured using a spectrophotometer. Whereafter, we reverse-transcribed 1 μg of RNA into cDNA (Vazyme, R333-01). qPCR analysis was performed on the Analytik Jena qTOWER3G Real-Time PCR System using Mix (Vazyme, Q711-02). Target gene expression relative to GAPDH was quantified via the $2^{-\Delta\Delta Ct}$ method. The reaction mixture (total volume 20 μL contained: 10 μL of 2× NovoStart® Universal Fast SYBR qPCR SuperMix, 0.4 μL of forward primer (10 μM), 0.4 μL of reverse primer (10 μM), 1 μL of cDNA (diluted 1:5), and RNase-free water to 20 μL. The thermal cycling program was as follows: initial denaturation at 95°C for 10 min; followed by 40 cycles of denaturation at 95°C for 10 s, annealing at 60°C for 30 s, and extension at 72°C for 30 s; then a melt curve analysis was performed. Each sample was run in triplicate.

Colony formation assay

Cell cultures were dissociated (VivaCell, C3530-0500) and prepared into a cell suspension. We dispensed 400 cells into each well of a 6-well plate, followed by the addition of medium for growth. Plates were incubated at 37°C, with the medium being refreshed regularly and colony sizes monitored. Culturing was continued until a sufficient number of colonies had formed in each well (approximately 12 days). The colonies were then washed and fixed, followed by staining a 15-minute staining with 0.2% crystal violet. The colonies were examined with a microscope, and images were captured.

Chromatin immunoprecipitation (ChIP)

ChIP assays were conducted to validate the binding of HIF-1α to the hypoxia response elements (HREs) within the promoters of SCAF1 using a Pierce Magnetic ChIP Kit (Thermo, 25157). Cells overexpressing HIF-1α were pretreated with 1% formaldehyde to crosslink protein-DNA complexes, followed by glycine quenching to a final concentration of 125 mM. Whereafter, the cells were lysed on ice. Chromatin was further digested with MNase at 37°C, and subsequently subjected to sonication to generate chromatin fragments of 200-1000 bp. Fragmented chromatin was incubated overnight at 4°C with the HIF-1α antibody, and then, incubated with protein A+G beads (preadsorbed with salmon sperm DNA) for 2 h at 4°C. Immune complexes were washed according to the protocol. Crosslinks were reversed by incubation at 65°C, and DNA was purified using the purification kit (QIAGEN). qPCR analysis was performed to quantify the enrichment of SCAF1 promoter regions. Non-specific IgG antibody from the same species served as a negative control.

Dual-luciferase reporter assay

To investigate the role of HREs in the SCAF1 and CLPP promoters in mediating HIF-1α-dependent transcriptional regulation, we performed dual-luciferase reporter assays and introduced site-directed mutations into the HRE sequences. The SCAF1 promoter region (promoter-1 or promoter-2) and its mutant variants (promoter-1-Mut1, -Mut2, and -Mut3), as well as the CLPP promoter region and its Mut1 and Mut2 variants, were cloned into the JS002 and JS0017 vectors, respectively, for luciferase reporter assays. Cells overexpressing HIF-1α were seeded into a 24-well plate pre-filled with Opti-MEM. The constructs were subsequently transfected into the cells separately using Lipofectamine 3000 (Invitrogen, L30000150). After 5 h, the medium was replaced with complete culture medium, and transfection was continued for 24 h. Luciferase activities were measured using the dual-Luciferase® Reporter Assay System (Promega, E1910).

Immunofluorescence

Cell smears were fixed. The cells were then immersed in 0.5% Triton X-100 solution (Amresco, X100) for 5 min, and then blocked with 3% BSA blocking solution (Servicebio, GC305010) for 30 minutes at room temperature to reduce non-specific binding. Primary antibodies were diluted as follows: Anti-LONP1 (Affinity, DF12119) at 1:250, Anti-COX7A2 (Affinity, AF9048) at 1:200, and Anti-SCAF1 (Affinity, AF9193) at 1:200. The cells were incubated overnight at 4°C with COX7A2 and SCAF1 or LONP1 antibodies. The corresponding fluorescent secondary antibodies were added and incubated for 2 h in the dark (Affinity, S0007) at 1:200. DAPI (Beyotime, C1002) was used for nuclear staining, and an anti-fade mounting medium (Beyotime, P0128M) was used to maintain the fluorescence on the slides. The results were observed and imaged under a fluorescence microscope.

Co-immunoprecipitation (Co-IP)

The Co-IP kit (Beyotime, P2197M) was used to validate the interactions between LONP1 and CLPP. Cells were resuspended in a pre-prepared lysis buffer, and centrifuged to collect the supernatant. Protein A+G beads were pre-incubated with Flag-Tag Antibody (Affinity, T0053) at room temperature. Subsequently, the antibody-coated beads were added to the protein lysate, and the mixture was incubated for 2 h at room temperature to allow immunoprecipitation. The antibody-bound protein complexes were then eluted using SDS-PAGE loading buffer and analyzed by Western blotting. Non-specific IgG antibodies from the same species served as negative controls.

GST pull-down

The Pierce™ GST Protein Interaction Pull-Down Kit (Thermo, 21516) was used to validate the interaction between COX7A2 and CLPP. The GST-tagged LONP1 was expressed in E. coli cells induced with 0.1 mM IPTG. Following cell lysis and centrifugation, the clarified lysate was loaded onto a pre-equilibrated Pierce™ Glutathione Spin Column and incubated at 4°C for 30 min to immobilize GST-LONP1. After washing, the resin was incubated with cell lysate overexpressing COX7A2 for 1 h at 4°C with gentle rotation. Bound complexes were eluted with 10 mM reduced glutathione, and eluates were resolved by SDS-PAGE and analyzed by Western blotting.

Xenograft tumor model

This animal experiment was approved by the Animal Experiment Ethics Committee of Jiangxi Medical College, Nanchang University (authorization number: CDYFY-IACUC-20240-8QR041). Nude mice (4-5 weeks) were used in this study and housed in a barrier environment maintained at 22-24°C with 40%-60% relative humidity, with free access to sterilized water and food. U251 cells expressing shSCAF1 or overexpressing COX7A2 were harvested using trypsin and resuspended in physiological saline. The cell concentration was adjusted to 8×10^6 cells/mL, and each mouse received subcutaneous injections of 100 μL of this cell suspension into the flank. Starting from day seven post-inoculation, tumor volumes were measured weekly using calipers according to the formula: (length × width^2)/2. After 4 weeks, mice were euthanized using CO_2, and tumor tissues were collected, weighed, and processed for WB and ATP analyses.

Statistical analysis

The gray value analysis was performed using Image J software (version 1.48v). Quantitative data were collected from a minimum of independent biological replicates and are presented as mean ± SD. Data analysis was carried out using GraphPad Prism (8.0.1). Comparisons between two groups were performed using an unpaired two tailed Student's t-test. Three or more group comparisons were made using One-Way ANOVA with Tukey's post hoc test, for multiple comparisons involving a time variable (e.g., cell viability at different days, tumor volume measured repeatedly), two-way repeated-measures ANOVA was used. Statistical significance was considered when the *P*-value was less than 0.05.

Results

Hypoxia promoted an increase in cell activity, migration, invasion and ATP level of glioma cells

First, we investigated the impact of hypoxia on cell biological behavior. Our findings demonstrated that $CoCl_2$ significantly increased cell viability (**Figure 1A**). Additionally, $CoCl_2$ was found to enhance cell motility and invasion of both A172 and U251 cells (**Figure 1B** and **1C**).

Then, we investigated the impact of hypoxia on ATP production in cells. $CoCl_2$ treatment led to a rise in ATP concentration (**Figure 1D**). Furthermore, the expression levels of SCAF1 and COX7A2 were examined, demonstrating that $CoCl_2$ triggered an increase in SCAF1 protein levels and a decrease in COX7A2 protein levels in A172 and U251 cells (**Figure 1E**).

Hypoxia promoted the increase of ATP level and respirasomes (CI+CIII$_2$+CIV) in glioma cells

HIF-1α mRNA and protein levels were increased by $CoCl_2$ treatment in A172 and U251 cells (**Figure 2A** and **2B**). Subsequently, we examined how HIF-1α affected ATP production and the formation of I+III$_2$+IV supercomplexes. U251 cells were genetically modified to overexpress HIF-1α (**Figure 2C** and **2D**). HIF-1α overexpression increased SCAF1 protein levels and reduced COX7A2 protein levels (**Figure 2E**). HIF-1α overexpression also elevated ATP levels in U251 cells (**Figure 2F**). Additionally, supercomplex formation was observed using BN-PAGE, showing that HIF-1α overexpression boosted the I+III$_2$+IV supercomplex formation in U251 cells (**Figure 2G**). Concurrently, a significant increase in basal OCR was observed in the HIF-1α-overexpression group, whereas there was no significant change in ECAR (**Figure 2H**, **2I**). The red/green fluorescence intensity ratio was also significantly elevated in the HIF-1α-overexpression group, indicating an increase in mitochondrial membrane potential (**Figure 2J**). Following treatment with the ATP synthase inhibitor oligomycin, OCR levels

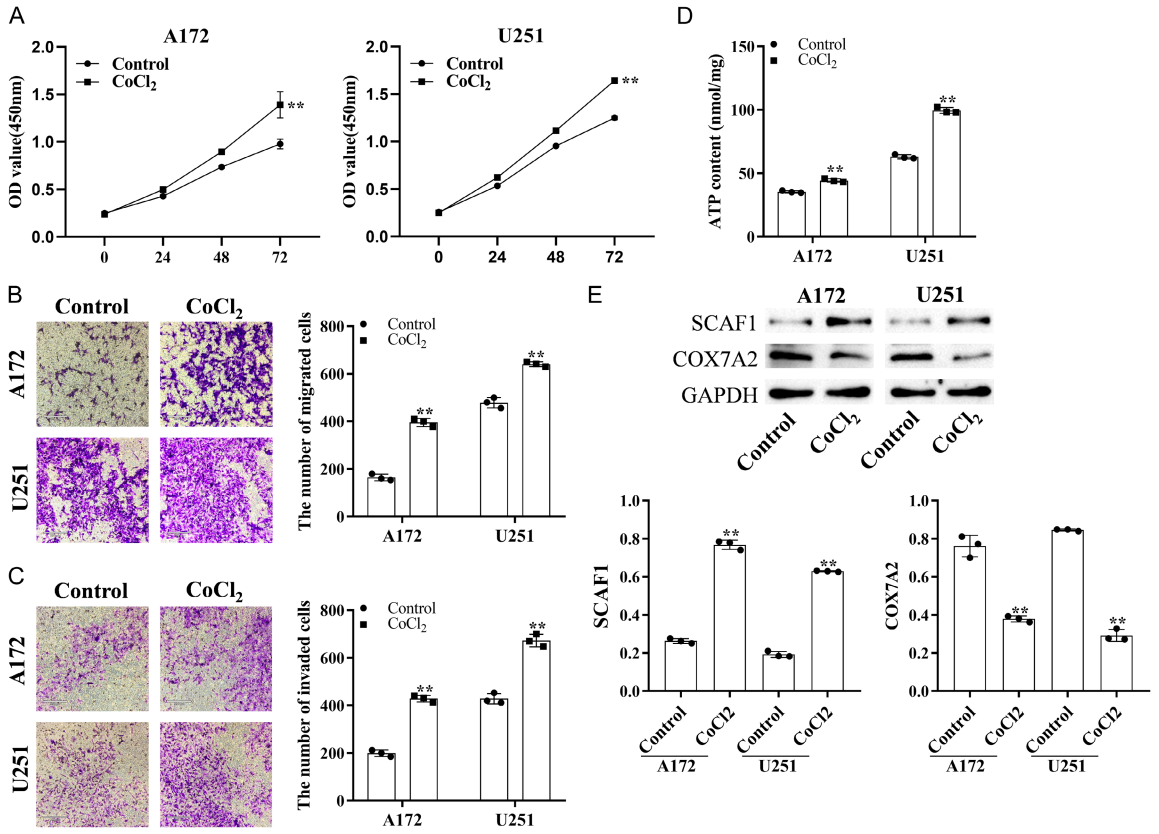

Figure 1. Hypoxia promoted an increase in cell activity, migration, invasion and of ATP level in glioma cells. A. The effect of $CoCl_2$ on cell viability was detected using the MTS assay. B, C. The effects of $CoCl_2$ on cell migration and invasion were detected using the Transwell assay, magnification: ×200. D. The effect of $CoCl_2$ on ATP concentration in A172 and U251 cells. E. WB was used to determine the expression levels of SCAF1 and COX7A2. Data are presented as mean ± SD from three independent experiments. Statistical analysis was performed using an unpaired two-tailed Student's t-test. $^{**}P < 0.01$, compared with Control group.

decreased. Following treatment with the OXPHOS uncoupler CCCP, the red-to-green fluorescence intensity ratio decreased significantly. These results suggest that the HIF-1α-induced increase in ATP levels is primarily attributable to enhanced oxidative phosphorylation rather than glycolysis.

COX7A2 knockdown promoted cell activity, clone formation, migration, invasion and the increase of ATP in glioma cells

The effect of COX7A2 knockdown on biological behavior and ATP generation of in U251 cells was investigated. U251 cells were engineered to have reduced expression of COX7A2, as shown in **Figure 3A** and **3B**. We selected the U251 cells of sh-COX7A2-1 for the subsequent experiments. This knockdown resulted in increased cell viability and clone formation of U251 cells (**Figure 3C** and **3D**). In addition, the reduced levels of COX7A2 were found to augment cell dissemination and invasion capabilities of U251 cells (**Figure 3E** and **3F**). Furthermore, the knockdown of COX7A2 led to an increase in the concentration of ATP within U251 cells (**Figure 3G**). To further examine the impact of COX7A2 knockdown on cellular respiration, the supercomplexes were analyzed using BN-PAGE. It was observed that downregulation of COX7A2 promoted the formation of $I+III_2+IV$ (**Figure 3H**).

HIF-1α targeted the SCAF1 promoter to regulate the expression level of SCAF1

We discovered multiple hypoxia-response elements (HREs) on the promoter of SCAF1. ChIP experiment demonstrated under hypoxic conditions, HIF-1α bound to the promoter of SCAF1 (**Figure 4A**). We then divided the SCAF1 promoter region into two parts (SCAF1-1 and

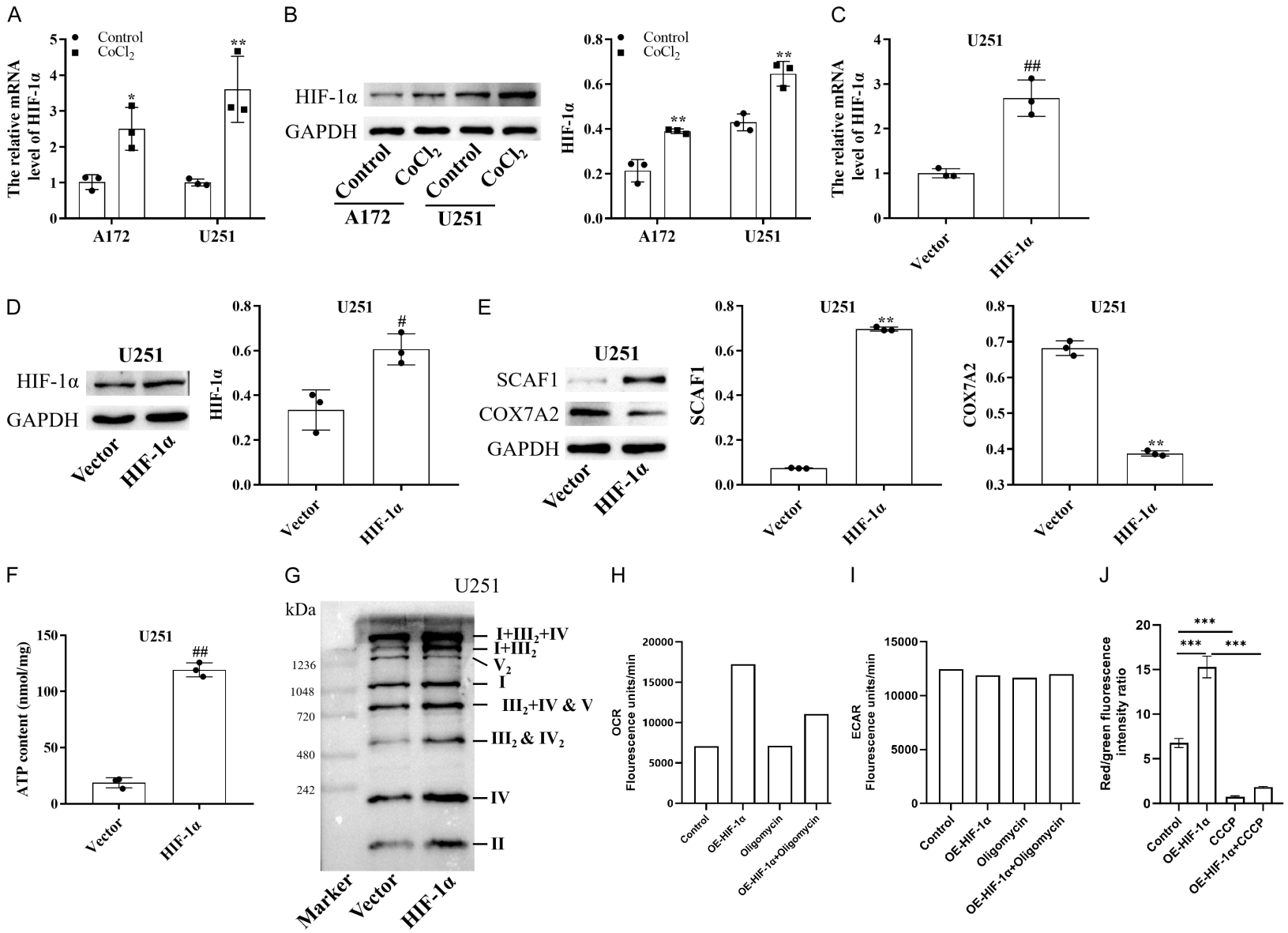

Figure 2. Overexpression of HIF-1α promoted the increase of ATP and respirasomes (CI+CIII$_2$+CIV) in A172 cells. A, B. RT-qPCR and western blot analysis were used to detect the expression of HIF-1α in A172 and U251 cells were treated with $CoCl_2$. C, D. RT-qPCR and western blot analysis were used to detect the expression of

HIF-1α in HIF-1α overexpression U251 cells. E. WB was used to detect the expression levels of SCAF1 and COX7A2 in HIF-1α overexpression U251 cells. F. The effect of HIF-1α on ATP concentration in U251 cells. G. Immunoblotting was performed on blue native polyacrylamide gel electrophoresis (BN-PAGE) gels in U251 cells with overexpressed HIF-1α. H, I. Changes in OCR and ECAR; the slope of the time interval during which the fluorescence value shows a linear trend is selected and used to indicate the magnitude of the change. J. Flow cytometry measurement of mitochondrial membrane potential. Data are presented as mean ± SD from three independent experiments. Statistical analysis was performed using an unpaired two-tailed Student's t-test. $^{**}P < 0.01$, compared with Control group; $^{**}P < 0.01$, compared with Vector group.

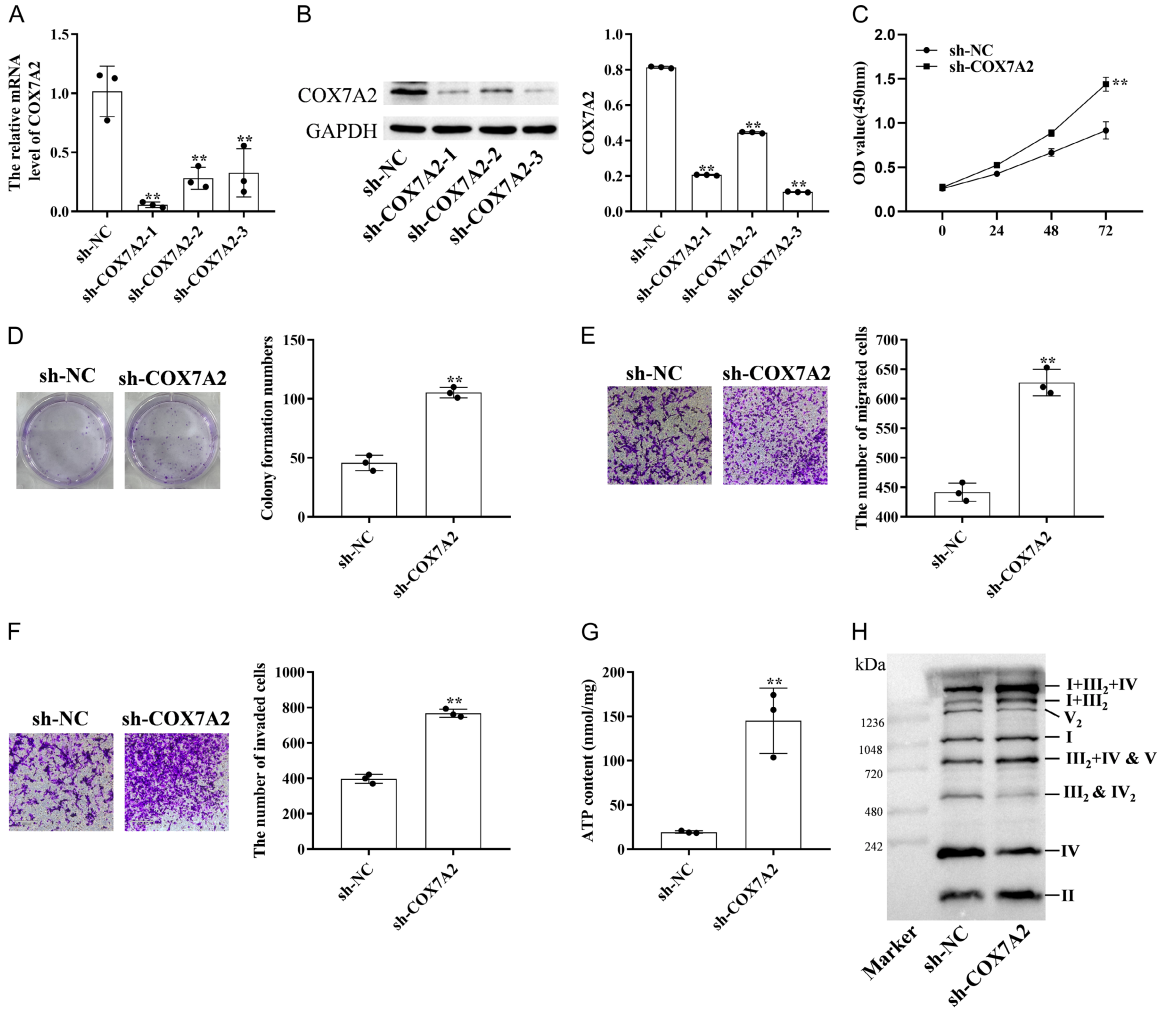

Figure 3. COX7A2 knockdown promoted cell activity, clone formation, migration, invasion and the increase of ATP in glioma cells. A, B. RT-qPCR and western blot analysis were used to detect the expression of COX7A2 in COX7A2 knockdown U251 cells. C. The effect of COX7A2 knockdown on cell viability was detected using the MTS assay. D. The effect of COX7A2 knockdown on cell proliferation was assessed through clonal formation assay, magnification: ×100. E, F. The effect of COX7A2 knockdown on cell migration and invasion was detected using the Transwell assay, magnification: ×200. G. The effects of COX7A2 knockdown on ATP concentration in U251 cells. H. Immunoblotting of blue native polyacrylamide gel electrophoresis (BN-PAGE) gel in COX7A2 knockdown U251 cells. Data are presented as mean ± SD from three independent experiments. Statistical analysis between the three or more groups was performed using one-way ANOVA followed by Tukey's HSD post-hoc test. Statistical analysis between two groups was performed using an unpaired two-tailed Student's t-test. C. Uses repeated measures analysis of variance. $^{**}P < 0.01$, compared with sh-NC group.

SCAF1-2), which both contain two GCGTGS and one ACGTG (**Table 1**). The dual-luciferase reporter test was then adopted, revealing that the SCAF1-1 region contained promoter binding

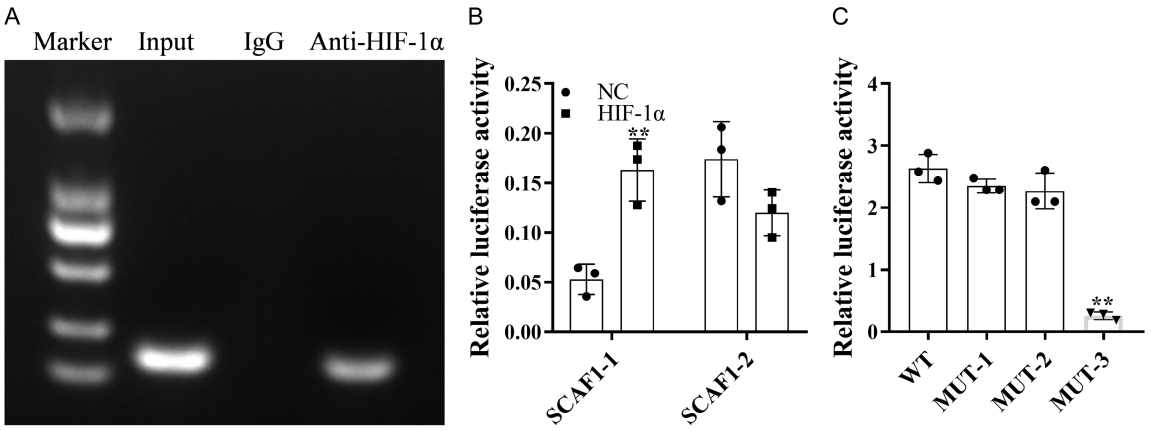

Figure 4. HIF-1α targeted the SCAF1 promoter to regulate the expression level of SCAF1. A. The ChIP experiment proved that HIF-1α binds to the SCAF1 promoter. B. Verify the promoter region of SCAF1 regulated by HIF-1α. C. Verify the predicted binding site. Data are presented as mean ± SD from three independent experiments. Statistical analysis between the three or more groups was performed using one-way ANOVA followed by Tukey's HSD post-hoc test. Statistical analysis between two groups was performed using an unpaired two-tailed Student's t-test. $^{**}P < 0.01$, compared with NC group, $^{**}P < 0.01$, compared with WT group.

sites (**Figure 4B**). Following this, we mutated two GCGTGS of SCAF1-1 to GTGCG (MUT-1 and MUT-2), and one ACGTG to CAGGT (MUT-3). Further analysis through dual luciferase reporter gene detection showed that MUT-3 significantly reduced luciferase activity (**Figure 4C**). This finding suggests that HIF-1α targets the promoter of SCAF1 and underpins in regulating the expression level of SCAF1.

Overexpression of SCAF1 promoted cell activity, clone formation, migration, invasion and the increase of ATP in glioma cells

Further investigation was carried out to study how overexpression of SCAF1 affected the biological behavior and ATP production of U251 cells. U251 cells were genetically modified to overexpress SCAF1 as shown in **Figure 5A** and **5B**, resulting in increased cell viability, clone formation (**Figure 5C** and **5D**). The migratory and invasive behavior of U251 cells were also increased by SCAF1 overexpression (**Figure 5E** and **5F**). In addition, overexpression of SCAF1 led to an increase in ATP concentration in U251 cells (**Figure 5G**). BN-PAGE analysis revealed an increased formation of $I+III_2+IV$ with overexpression of SCAF1, as depicted in **Figure 5H**.

HIF-1α regulated the expression of LONP1 to degrade COX7A2 in glioma cells

Absence of HRE sequences was observed in the COX7A2 promoter region. Thus, regulation of COX7A2 protein level by HIF-1α may involve alternative mechanisms. It has been unveiled that HIF-1α can target the LONP1 promoter to modulate its expression. Therefore, we proceeded to ask if LONP1 is implicated in the regulation of COX7A2 by HIF-1α. Initially, we examined if HIF-1α influenced LONP1 expression, revealing that its overexpression led to increased LONP1 (**Figure 6A** and **6B**). Subsequently, we generated U251 cells with LONP1 knockdown (**Figure 6C** and **6D**), and U251 cells in sh-LONP1-2 group were used for the subsequent experiments. We observed that LONP1 knockdown resulted in increased COX7A2 levels, suggesting LONP1's ability to regulate COX7A2 protein levels (**Figure 6E**).

Given LONP1's role in protein degradation, we further investigated whether LONP1 targeted COX7A2 to modulate its protein level. The results from both Co-IP assay and GST-pull experiments, indicated that LONP1 indeed targeted and regulated COX7A2 (**Figure 6F** and **6G**). These findings suggest that LONP1 may target and degrade COX7A2, thereby reducing its protein levels.

HIF-1α regulated the CLPP level to reduce the COX7A2 protein level in glioma cells

Since LONP1 and CLPP share many substrates, we constructed U251 cells with CLPP knockdown and overexpression (**Figure 7A-D**). Knockdown of CLPP increased, while overex-

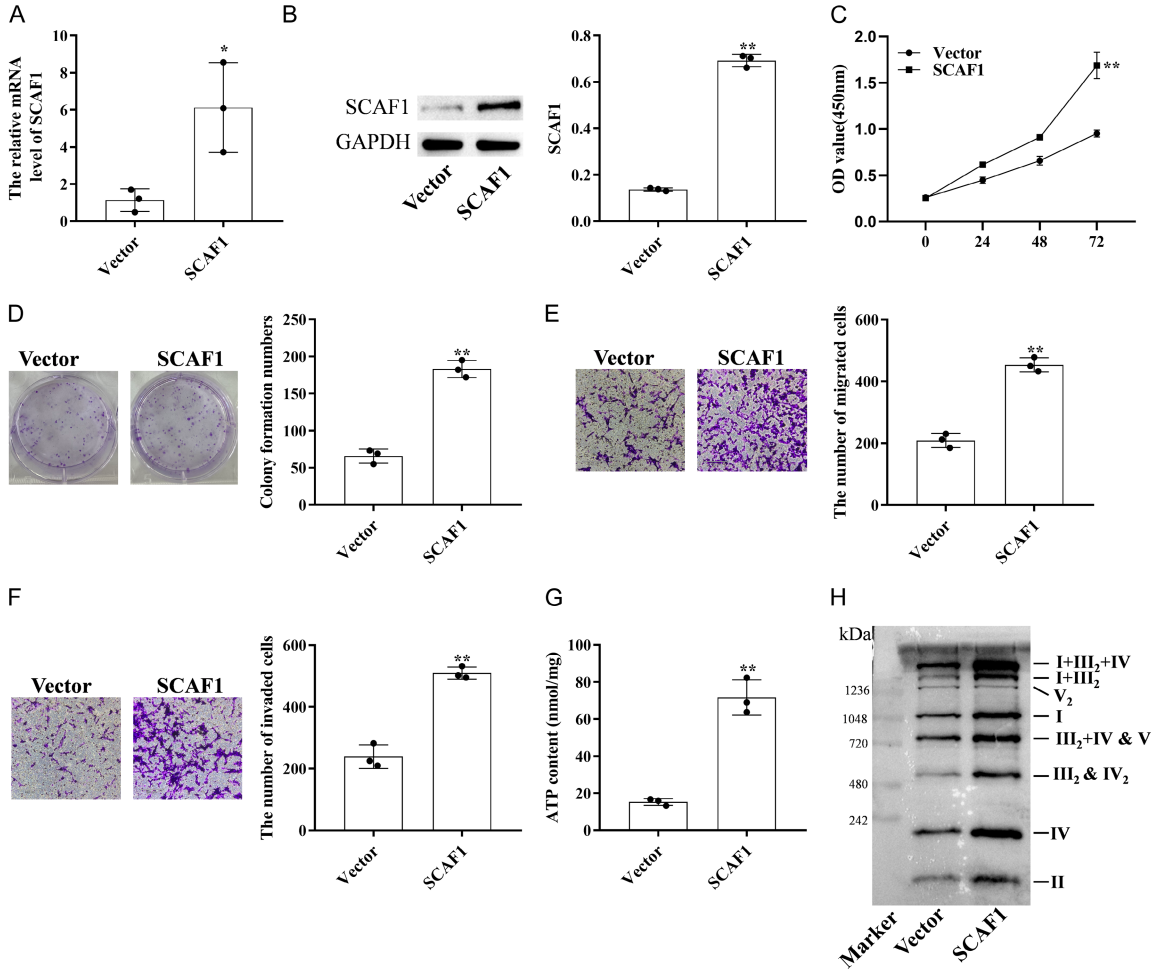

Figure 5. Overexpression of SCAF1 promoted cell activity, clone formation, migration, invasion and the increase of ATP in glioma cells. A, B. RT-qPCR and western blot analysis were used to detect the expression of SCAF1 in SCAF1 overexpression U251 cells. C. The effect of SCAF1 overexpression on cell viability was detected using the MTS assay in U251 cells. D. The effect of SCAF1 overexpression on cell proliferation was assessed through clonal formation assay in U251 cells, magnification: ×100. E, F. The effect of SCAF1 overexpression on cell migration and invasion was detected using the Transwell assay in U251 cells, magnification: ×100. G. The effects of SCAF1 overexpression on ATP concentration in U251 cells. H. Immunoblotting of blue native polyacrylamide gel electrophoresis (BN-PAGE) gel in SCAF1 overexpression U251 cells. Data are presented as mean ± SD from three independent experiments. Statistical analysis was performed using an unpaired two-tailed Student's t-test. C. Uses repeated measures analysis of variance. $^{**}P < 0.01$, compared with Vector group.

pression of CLPP reduced the expression level of COX7A2 (**Figure 7E**). Due to CLPP's protein degradation effect, we further explored whether CLPP targets COX7A2 to regulate its protein level. Both the Co-IP experiment and the GST-pull down assay proved that CLPP targets and regulates COX7A2 (**Figure 7F** and **7G**), suggesting that CLPP may degrade COX7A2 to reduce its protein level.

We then investigated whether HIF-1α regulates CLPP expression. The results showed that overexpression of HIF-1α significantly increased CLPP expression (**Figure 8A** and **8B**). Next, we examined whether HIF-1α directly targets the CLPP promoter to regulate its transcriptional activity. Bioinformatic analysis identified two HREs motifs within the CLPP promoter region. To verify whether HIF-1α targets and regulates the CLPP promoter, a dual-luciferase reporter gene assay was performed. Surprisingly, the results indicated that HIF-1α did not influence the transcription of CLPP by targeting its promoter (**Figure 8C**). Therefore, HIF-1α might regulate the expression of CLPP through other mechanisms.

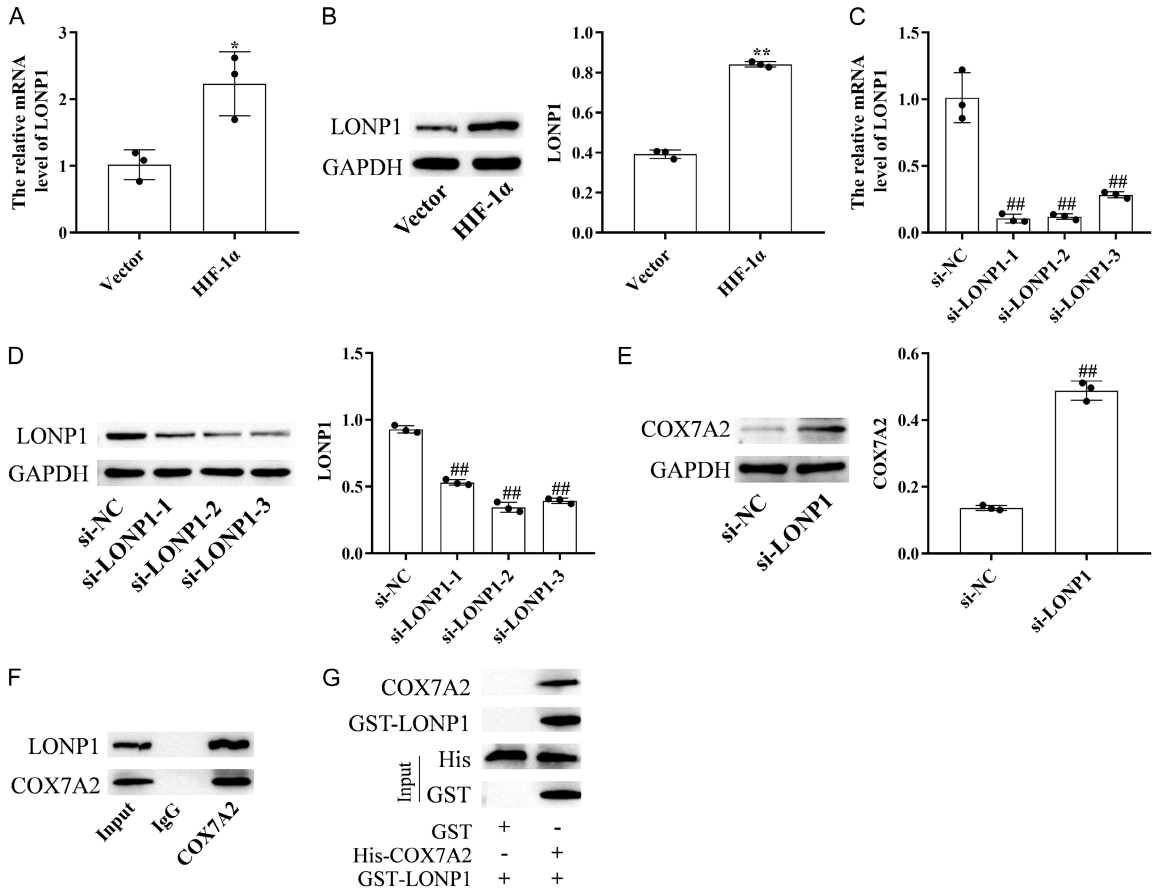

Figure 6. HIF-1α regulated the expression of LONP1 to degrade COX7A2 in U251 cells. A, B. RT-qPCR and western blot analysis were used to detect the expression of LONP1 in HIF-1α overexpression U251 cells. C, D. RT-qPCR and western blot analysis were used to detect the expression of LONP1 in LONP1 knockdown U251 cells. E. RT-qPCR and western blot analysis were used to detect the expression of COX7A2 in LONP1 knockdown U251 cells. F. CoIP analysis of interaction between LONP1 and COX7A2. G. GST pull-down analysis of interaction between LONP1 and COX7A2. Data are presented as mean ± SD from three independent experiments. Statistical analysis between the three or more groups was performed using one-way ANOVA followed by Tukey's HSD post-hoc test. Statistical analysis between two groups was performed using an unpaired two-tailed Student's t-test. $^{**}P < 0.01$, compared with Vector group; $^{\#\#}P < 0.01$, compared with sh-NC group.

Knockdown of SCAF1 or overexpression of COX7A2 inhibited tumor formation in nude mice

Finally, a xenograft tumor model in nude mice was established using U251 cells with SCAF1 knockdown or COX7A2 overexpression. The results showed that SCAF1 protein levels were significantly reduced in tumor tissues from the shSCAF1 group ($P < 0.001$), indicating that the shSCAF1 lentivirus effectively knocked down SCAF1 in vivo (**Figure 9A**). Conversely, COX7A2 protein levels were significantly elevated in tumor tissues from the COX7A2 OE group ($P < 0.001$), confirming the successful overexpression of COX7A2 in vivo (**Figure 9B**). Knocking down SCAF1 reduces the volume and weight of the tumor (**Figure 9A-E**). On the other hand, overexpression of COX7A2 reduces the volume and weight of the tumor. Additionally, knocking down SCAF1 has been found to reduce the concentration of ATP, whereas overexpression of COX7A2 has the opposite effect on tumor formation in nude mice (**Figure 9F**).

These findings suggest that HIF-1α promoted the degradation of COX7A2 by regulating LONP1 and CLLP, while also inducing an increase in the expression of SCAF1 by targeting its promoter. This resulted in an increase in the replacement of COX7A2 with SCAF1, ultimately promoting ATP generation and furthering glioma progression (**Figure 10**).

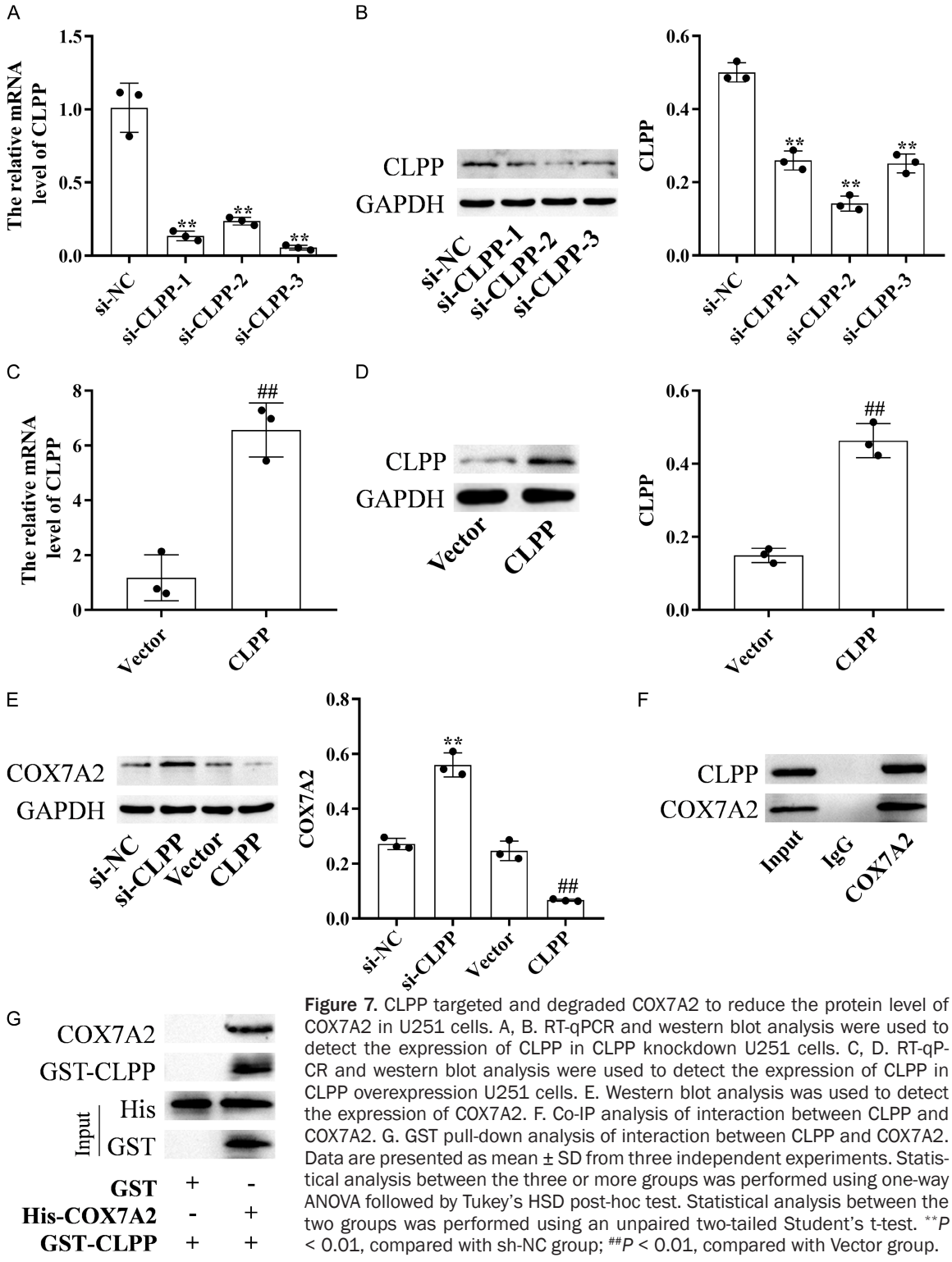

Figure 7. CLPP targeted and degraded COX7A2 to reduce the protein level of COX7A2 in U251 cells. A, B. RT-qPCR and western blot analysis were used to detect the expression of CLPP in CLPP knockdown U251 cells. C, D. RT-qPCR and western blot analysis were used to detect the expression of CLPP in CLPP overexpression U251 cells. E. Western blot analysis was used to detect the expression of COX7A2. F. Co-IP analysis of interaction between CLPP and COX7A2. G. GST pull-down analysis of interaction between CLPP and COX7A2. Data are presented as mean ± SD from three independent experiments. Statistical analysis between the three or more groups was performed using one-way ANOVA followed by Tukey's HSD post-hoc test. Statistical analysis between the two groups was performed using an unpaired two-tailed Student's t-test. $^{**}P < 0.01$, compared with sh-NC group; $^{\#\#}P < 0.01$, compared with Vector group.

Discussion

Glioma often presents with hypoxia as a common pathological feature. The level of hypoxia in glioma is correlated with the grade of the tumor [33]. Up-regulating the HIF family in glioma cells is promoted by the hypoxic microenvironment, leading to their aggressive phenotype

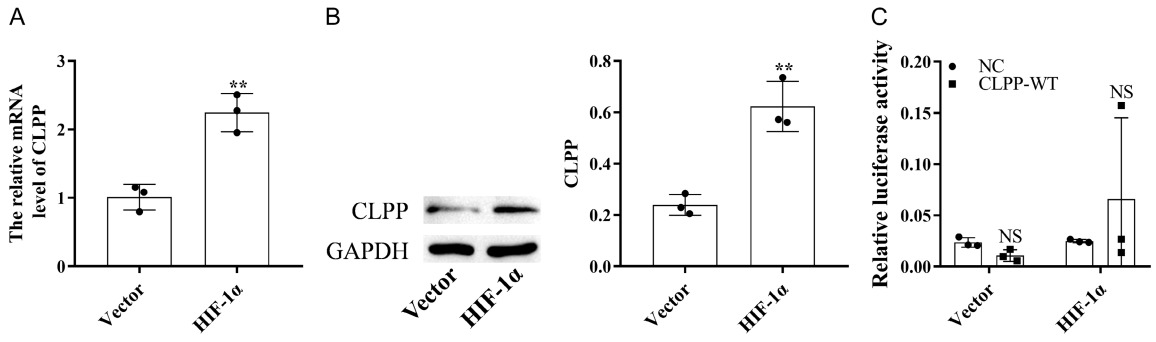

Figure 8. HIF-1α increased the level of CLPP but not by targeting the CLPP promoter. A, B. RT-qPCR and western blot analysis were used to detect the expression of CLPP in HIF-1α overexpression U251 cells. C. Dual-luciferase reporter gene assay. Data are presented as mean ± SD from three independent experiments. Statistical analysis was performed using an unpaired two-tailed Student's t-test. $^{**}P < 0.01$, compared with Vector group.

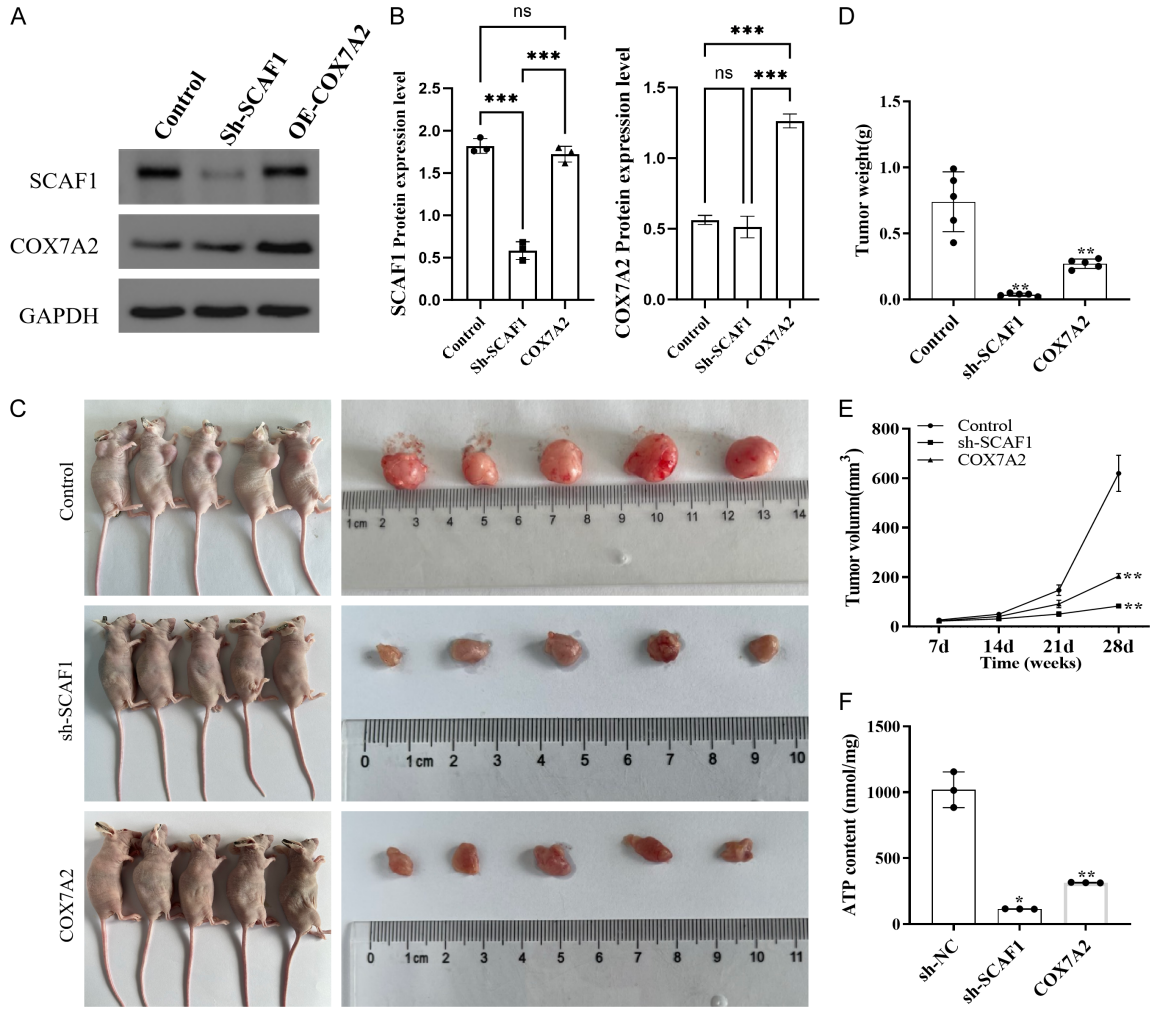

Figure 9. Knockdown of SCAF1 or overexpression of COX7A2 inhibited tumor formation in nude mice. A, B. Western blot analysis was used to detect the expression of SCAF1 and COX7A2 in tumor tissues. C. Representative images of tumors, magnification: ×200. D, E. Tumor volume and weight. F. ATP concentration. Data are presented as mean ± SD from three independent experiments. Statistical analysis was performed using one-way ANOVA followed by Tukey's HSD post-hoc test. C. Uses repeated measures analysis of variance. $^{*}P < 0.05$, compared with Control group; $^{**}P < 0.01$, compared with Control group.

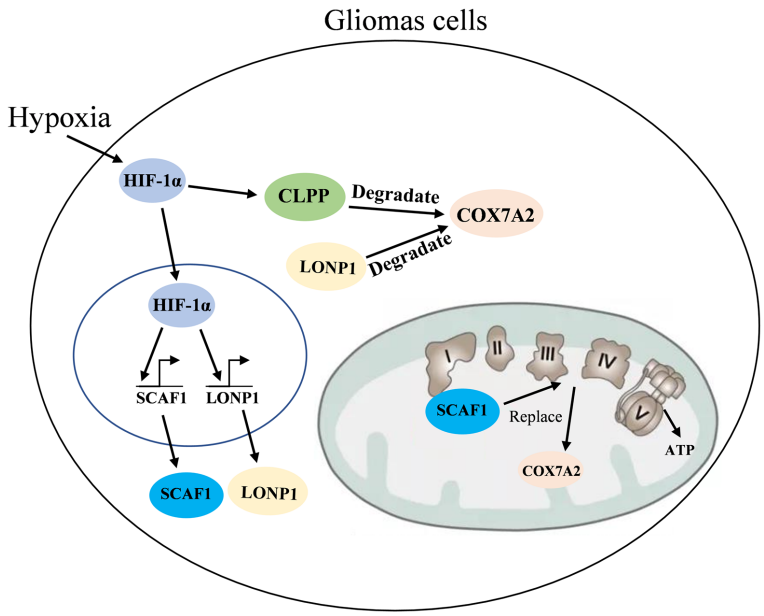

Figure 10. HIF-1α regulated COX7A2 and SCAF1 expression to upregulate ATP levels in glioma cells.

[34-37]. HIF-1 has been widely recognized as a regulator of glioma progression by promoting hypoxia [38]. A study by Lee et al. found that $CoCl_2$ can effectively mimic the molecular effects of true hypoxia and serves as an easy-to-use, stable and controllable platform for simulating hypoxia [39]. HIF-1α has a critical role in determining cancer outlook, with diverse impacts on angiogenesis, cell invasion, metastasis, survival, and metabolic alterations [40, 41]. Hypoxic exposure upregulated HIF-1α expression and enhanced various cellular processes such as viability, colony formation, migration, and invasion. In conditions of natural serine/glycine (S/G) deprivation, HIF-1α-induced expression of glycolysis-related genes encourages glucose absorption, glycolysis, and glycolytic flow, supporting the de novo serine synthesis pathway (SSP) in GBM cells, which aids in the survival and rapid proliferation of tumor cells [42]. Regarding metabolic regulation, HIF-1α induced an increase in cellular ATP and changes in SCs. The study also found that the baseline OCR and mitochondrial membrane potential in the HIF-1α-overexpression group were significantly higher than those in the control group, whilst there was no significant change in ECAR. Oligomycin completely blocked the increase in OCR caused by HIF-1α overexpression, and CCCP also eliminated the increase in membrane potential, suggesting that HIF-1α regulates mitochondrial oxidative phosphorylation.

SCs can have various subtypes depending on the organism, metabolic status, and tissue type [20, 43]. Mammalian SCs are typically made up of combinations such as $CIII_2$+CIV, CI+$CIII_2$, CI+$CIII_2$+CIV, and CI+$CIII_2$+CIV_{2-n} [44]. The SCs These SCs, which include complex I, Complex III dimers, and one or more copies of complex IV, are also known as "respirasomes (CI+$CIII_2$+CIV)" because they have the ability to transfer electrons from NADH to molecular oxygen independently, allowing them to "breathe" [45-47]. Therefore, it is important to understand how HIF-1α influences changes in SCs. This study revealed that HIF-1α controls the expression of COX7A2 and SCAF1. Downregulating COX7A2 and upregulating SCAF1 led to increased ATP generation, the formation of respirasomes (CI+$CIII_2$+CIV), and a higher proportion of other SCs. Previous studies have reported that HIF-1α can enhance oxidative phosphorylation (OXPHOS), particularly under conditions where it promotes the assembly of mitochondrial supercomplexes [48]. ROS are generated as a result of inefficient OXPHOS, and they are neutralized by enzymes like catalase, peroxoreductin, and superoxide dismutase [49]. Failure to decrease the level of reactive oxygen species (ROS) may lead to its toxicity to cells, ultimately hindering cell survival. Supercomplexes play a vital role in stabilizing individual complexes and aiding in substrate transfer, which helps mitigate ROS production [43, 50, 51]. Therefore, HIF-1α-controlled SCAF1 and COX7A2 may be crucial in promoting ATP synthesis, reducing ROS levels, and safeguarding cells by influencing the structure and types of SCs.

How does HIF-1α control the expression of SCAF1 and COX7A2? It has been observed that COX7A2L expression increases in hypoxic conditions [52]. When a cell is in a state of hypoxia, HIF-1α accumulates gradually and moves to

the nucleus. Following this, HIF-1α binds with HIF-1β to create a stable complex that can bind to the HRE region of the target gene promoter [53]. In this research, HIF-1α directly influences the levels of SCAF1 by targeting the HRE in the SCAF1 gene promoter. While HIF-1α does not directly target COX7A2 gene promoters, it does impact COX7A2 levels through alternative mechanisms.

It has been demonstrated that hypoxia decreases the ATP-dependent activity of LONP1 and/or CLPP, resulting in the accumulation of mitochondrial transcripts [28]. Our research also showed that HIF-1α can target the HRE promoter to regulate CLPP levels and LONP1 gene expression. A previous study demonstrated that HIF-1α was able to target the promoter of the LONP1 gene in order to control the expression of LONP1 [26]. Moreover, both CLPP and LONP1 can regulate COX7A2 levels by targeting its promoter. Therefore, HIF-1α directly modulates the energy metabolism of mitochondria by targeting the promoters of LONP1 and CLPP, impacting glioma progression. LONP1 and CLPP RNA expression is significantly increased in various human cancers, with similar patterns across different cancer types [27]. Elevated levels of LONP1 are associated with a poor prognosis [54]. LONP1 and CLPP play a crucial role in regulating mitochondrial function and OXPHOS in tumor cells. In response to HIF1a, LONP1 targets COX4-1 for degradation and facilitates its replacement with the more efficient COX4-2 subunit under low oxygen conditions [26]. LonP1 is upregulated under stress conditions, like hypoxia, in tumors and phosphorylated by Akt to enhance its protease activity, promoting oxidative metabolism and tumor cell metastasis [55]. Inhibition of CLPP in leukemia cells results in reduced oxidative phosphorylation, mitochondrial metabolism, and cell death [56]. Additionally, CLPP inhibition leads to dysregulation of mitochondrial respiratory capacity, activation of cell stress, decreased cell proliferation, and impaired metastasis and transmission [57, 58]. Combining inhibition of LONP1 and CLPP increases unfolded SHMT2 protein levels and enhances sensitivity to SHMT2 inhibitors, producing an environment in which cell growth waned and cell death rose under metabolic stress [27, 59]. However, this study lacked direct evidence of proteolytic degradation to demonstrate that LONP1/CLPP directly cleaves COX7A2. Therefore, we currently define COX7A2 as a candidate substrate for LONP1/CLPP. Future studies should establish an in vitro degradation system using purified recombinant proteases and substrates or employ mitochondrial protease-specific inhibitors to track substrate accumulation to confirm this regulatory relationship.

Our previous research has indicated that high levels of COX7A2 are linked to a positive prognosis in glioma and act as an independent factor in predicting survival [14]. COX7A2 is a component of the final part of the mitochondrial respiratory chain complex IV, known as cytochrome c oxidase [60, 61]. Studies in zebrafish and mice have suggested that SCAF1 may improve metabolic efficiency [48]. Overexpression of SCAF1 in breast and endometrial cancer cells has been shown to enhance growth both in the lab and in living organisms, stabilize mitochondrial supercomplex formation even in low oxygen conditions, and increase tolerance to hypoxia [62]. Lower levels of SCAF1 result in decreased ATP levels, with a particular impact on mitochondrial efficiency in low oxygen environments [52]. The findings of experiments conducted in vitro and in vivo in this study demonstrated that reducing COX7A2 and increasing SCAF1 resulted in higher ATP production, the development of respirasomes ($CI+CIII_2+CIV$), and a larger proportion of other supercomplexes.

How do COX7A2 and SCAF1 impact the formation and composition of the SCs in the electron transport chain? SCAF1 plays a vital role in promoting the interaction between complex III and complex IV, which is necessary for creating respirasomes ($CI+CIII_2+CIV$) [20, 63]. The study has shown that the absence of SCAF1 hinders the incorporation of complex IV into the SC structure, while its presence allows for the formation of different SC configurations with complex IV [64]. However, these findings have also been disputed [65-67]. Research suggests that human SCAF1 primarily binds to free complex III, enhancing the stability of the III_2+IV supercomplex without affecting the formation of respirasomes ($CI+CIII_2+CIV$) [65]. Most respirasomes ($CI+CIII_2+CIV$), contain COX7A2, but a significant portion (30-40%) of them in human cells depend on SCAF1 [15]. Therefore, under hypoxic conditions, increased

SCAF1 expression and reduced levels of COX7A2 result in the substitution of COX7A2 with SCAF1, which facilitates I+III_2+IV assembly.

There are some limitations to this study. The limited animal sample size and lack of clinical data restricted the generalizability and clinical relevance of the findings. Due to various constraints, BN-PAGE was not completed in the in vivo tissue samples. This study is the absence of direct rescue experiments, such as re-expressing COX7A2 or knocking down SCAF1 in HIF-1α-overexpressing cells to observe phenotypic reversal. Future studies should definitively validate the functional necessity of this axis by establishing conditional co-expression systems or conducting CRISPRa/i-based rescue experiments. Additionally, the study only focused on the impact of HIF-1α on oxidative phosphorylation and did not provide a comprehensive assessment of its effect on the overall metabolism of glioma cells. Furthermore, no screening or validation of potential therapeutic targets was conducted, and there was a lack of assessment of the clinical application prospects of these targets. Future studies should aim to validate these findings in in vivo models, increase sample sizes, integrate clinical data, elucidate the molecular mechanisms involved, and conduct metabolomics analyses and drug screening to gain a deeper understanding of HIF-1α's role in gliomas and to develop new treatment strategies.

Conclusion

In summary, this study identified the molecular mechanism by which HIF-1α influences the formation and composition of mitochondrial supercomplexes. This mechanism involves the regulation of SCAF1 and COX7A2, ultimately promoting the ATP production to regulate the progression of glioma cells. These findings offer a new perspective on understanding metabolic reprogramming in the hypoxic microenvironment of gliomas and present a potential target for developing novel therapeutic strategies for this type of cancer.

Acknowledgements

This work was supported by the National Natural Science Foundation of China (Grant No.: 82160525).

Disclosure of conflict of interest

None.

Address correspondence to: Shengze Deng, Department of Neurosurgery, The First Affiliated Hospital, Jiangxi Medical College, Nanchang University, No. 17 Yongwai Zheng Street, Nanchang 330006, Jiangxi, China. Tel: +86-18679155751; E-mail: ndyfy03417@ncu.edu.cn

References

[1] Ostrom QT, Bauchet L, Davis FG, Deltour I, Fisher JL, Langer CE, Pekmezci M, Schwartzbaum JA, Turner MC, Walsh KM, Wrensch MR and Barnholtz-Sloan JS. The epidemiology of glioma in adults: a "state of the science" review. Neuro Oncol 2014; 16: 896-913.

[2] Miller KD, Ostrom QT, Kruchko C, Patil N, Tihan T, Cioffi G, Fuchs HE, Waite KA, Jemal A, Siegel RL and Barnholtz-Sloan JS. Brain and other central nervous system tumor statistics, 2021. CA Cancer J Clin 2021; 71: 381-406.

[3] Stupp R, van den Bent MJ and Hegi ME. Optimal role of temozolomide in the treatment of malignant gliomas. Curr Neurol Neurosci Rep 2005; 5: 198-206.

[4] Dubrow R, Darefsky AS, Jacobs DI, Park LS, Rose MG, Laurans MS and King JT Jr. Time trends in glioblastoma multiforme survival: the role of temozolomide. Neuro Oncol 2013; 15: 1750-1761.

[5] Kozakiewicz P, Grzybowska-Szatkowska L, Ciesielka M, Całka P, Osuchowski J, Szmygin P, Jarosz B, Ostrowska-Leśko M, Dudka J, Tkaczyk-Wlizło A and Ślaska B. Mitochondrial DNA changes in respiratory complex I genes in brain gliomas. Biomedicines 2023; 11: 1183.

[6] Hwang HJ, Lynn SG, Vengellur A, Saini Y, Grier EA, Ferguson-Miller SM and LaPres JJ. Hypoxia inducible factors modulate mitochondrial oxygen consumption and transcriptional regulation of nuclear-encoded electron transport chain genes. Biochemistry 2015; 54: 3739-3748.

[7] Sancho P, Barneda D and Heeschen C. Hallmarks of cancer stem cell metabolism. Br J Cancer 2016; 114: 1305-1312.

[8] Bryant NL, Gillespie GY, Lopez RD, Markert JM, Cloud GA, Langford CP, Arnouk H, Su Y, Haines HL, Suarez-Cuervo C and Lamb LS Jr. Preclinical evaluation of ex vivo expanded/activated γδ T cells for immunotherapy of glioblastoma multiforme. J Neurooncol 2011; 101: 179-188.

[9] Caruana NJ and Stroud DA. The road to the structure of the mitochondrial respiratory

chain supercomplex. Biochem Soc Trans 2020; 48: 621-629.
[10] Chen L, Xin ZC, Li X, Tian L, Yuan YM, Liu G, Jiang XJ and Guo YL. Cox7a2 mediates steroidogenesis in TM3 mouse leydig cells. Asian J Androl 2006; 8: 589-594.
[11] Rönn T, Poulsen P, Hansson O, Holmkvist J, Almgren P, Nilsson P, Tuomi T, Isomaa B, Groop L, Vaag A and Ling C. Age influences DNA methylation and gene expression of COX7A1 in human skeletal muscle. Diabetologia 2008; 51: 1159-1168.
[12] Elsner M, Rauser S, Maier S, Schöne C, Balluff B, Meding S, Jung G, Nipp M, Sarioglu H, Maccarrone G, Aichler M, Feuchtinger A, Langer R, Jütting U, Feith M, Küster B, Ueffing M, Zitzelsberger H, Höfler H and Walch A. MALDI imaging mass spectrometry reveals COX7A2, TAGLN2 and S100-A10 as novel prognostic markers in Barrett's adenocarcinoma. J Proteomics 2012; 75: 4693-4704.
[13] Ma X, Ligan C, Huang S, Chen Y, Li M, Cao Y, Zhao W and Zhao S. Mitochondrial activity related genes of mast cells identify poor prognosis and metastasis of ovarian cancer. Immunobiology 2024; 229: 152831.
[14] Deng S, Li Y, Yi G, Lei B, Guo M, Xiang W, Chen Z, Liu Y and Qi S. Overexpression of COX7A2 is associated with a good prognosis in patients with glioma. J Neurooncol 2018; 136: 41-50.
[15] Fernández-Vizarra E, López-Calcerrada S, Formosa LE, Pérez-Pérez R, Ding S, Fearnley IM, Arenas J, Martín MA, Zeviani M, Ryan MT and Ugalde C. SILAC-based complexome profiling dissects the structural organization of the human respiratory supercomplexes in SCAFI(KO) cells. Biochim Biophys Acta Bioenerg 2021; 1862: 148414.
[16] Schägger H and Pfeiffer K. Supercomplexes in the respiratory chains of yeast and mammalian mitochondria. EMBO J 2000; 19: 1777-1783.
[17] Guo R, Zong S, Wu M, Gu J and Yang M. Architecture of human mitochondrial respiratory megacomplex I(2)III(2)IV(2). Cell 2017; 170: 1247-1257.e1212.
[18] Greggio C, Jha P, Kulkarni SS, Lagarrigue S, Broskey NT, Boutant M, Wang X, Conde Alonso S, Ofori E, Auwerx J, Cantó C and Amati F. Enhanced respiratory chain supercomplex formation in response to exercise in human skeletal muscle. Cell Metab 2017; 25: 301-311.
[19] Azuma K, Ikeda K and Inoue S. Functional mechanisms of mitochondrial respiratory chain supercomplex assembly factors and their involvement in muscle quality. Int J Mol Sci 2020; 21: 3182.
[20] Cogliati S, Calvo E, Loureiro M, Guaras AM, Nieto-Arellano R, Garcia-Poyatos C, Ezkurdia I, Mercader N, Vázquez J and Enriquez JA. Mechanism of super-assembly of respiratory complexes III and IV. Nature 2016; 539: 579-582.
[21] Kaur B, Khwaja FW, Severson EA, Matheny SL, Brat DJ and Van Meir EG. Hypoxia and the hypoxia-inducible-factor pathway in glioma growth and angiogenesis. Neuro Oncol 2005; 7: 134-153.
[22] Vengellur A, Woods BG, Ryan HE, Johnson RS and LaPres JJ. Gene expression profiling of the hypoxia signaling pathway in hypoxia-inducible factor 1alpha null mouse embryonic fibroblasts. Gene Expr 2003; 11: 181-197.
[23] Ratcliffe PJ. Oxygen sensing and hypoxia signalling pathways in animals: the implications of physiology for cancer. J Physiol 2013; 591: 2027-2042.
[24] Patrick S and Sen E. Mitochondria and redox homeostasis - the backseat drivers in glioma. Free Radic Res 2025; 59: 557-569.
[25] Vengellur A and LaPres JJ. The role of hypoxia inducible factor 1alpha in cobalt chloride induced cell death in mouse embryonic fibroblasts. Toxicol Sci 2004; 82: 638-646.
[26] Fukuda R, Zhang H, Kim JW, Shimoda L, Dang CV and Semenza GL. HIF-1 regulates cytochrome oxidase subunits to optimize efficiency of respiration in hypoxic cells. Cell 2007; 129: 111-122.
[27] Lee YG, Kim HW, Nam Y, Shin KJ, Lee YJ, Park DH, Rhee HW, Seo JK and Chae YC. LONP1 and ClpP cooperatively regulate mitochondrial proteostasis for cancer cell survival. Oncogenesis 2021; 10: 18.
[28] Sun CL, Van Gilst M and Crowder CM. Hypoxia-induced mitochondrial stress granules. Cell Death Dis 2023; 14: 448.
[29] Hou Y, Zhang Y, Jiang S, Xie N, Zhang Y, Meng X and Wang X. Salidroside intensifies mitochondrial function of CoCl(2)-damaged HT22 cells by stimulating PI3K-AKT-MAPK signaling pathway. Phytomedicine 2023; 109: 154568.
[30] Fusagawa H, Sato T, Yamada T, Naito A, Tokuda N, Yamauchi N, Ichise N, Ogawa T, Karaushi T, Teramoto A and Tohse N. High-intensity interval training using electrical stimulation ameliorates muscle fatigue in chronic kidney disease-related cachexia by restoring mitochondrial respiratory dysfunction. Front Physiol 2024; 15: 1423504.
[31] Said HM, Hagemann C, Stojic J, Schoemig B, Vince GH, Flentje M, Roosen K and Vordermark D. GAPDH is not regulated in human glioblastoma under hypoxic conditions. BMC Molecular Biology 2007; 8: 55.
[32] Said HM, Polat B, Hagemann C, Anacker J, Flentje M and Vordermark D. Absence of GAPDH regulation in tumor-cells of different origin

under hypoxic conditions in - vitro. BMC Res Notes 2009; 2: 8.
[33] Evans SM, Judy KD, Dunphy I, Jenkins WT, Hwang WT, Nelson PT, Lustig RA, Jenkins K, Magarelli DP, Hahn SM, Collins RA, Grady MS and Koch CJ. Hypoxia is important in the biology and aggression of human glial brain tumors. Clin Cancer Res 2004; 10: 8177-8184.
[34] Miska J, Lee-Chang C, Rashidi A, Muroski ME, Chang AL, Lopez-Rosas A, Zhang P, Panek WK, Cordero A, Han Y, Ahmed AU, Chandel NS and Lesniak MS. HIF-1α is a metabolic switch between glycolytic-driven migration and oxidative phosphorylation-driven immunosuppression of Tregs in glioblastoma. Cell Rep 2019; 27: 226-237.e224.
[35] Gabriely G, Wheeler MA, Takenaka MC and Quintana FJ. Role of AHR and HIF-1α in glioblastoma metabolism. Trends Endocrinol Metab 2017; 28: 428-436.
[36] Luo Z, Bai M, Xiao X, Zhang W, Liu X, Yang X, Li S, Huan Y, Wu Z, Zhang X and Cao W. Silencing of HIF-1α enhances the radiation sensitivity of human glioma growth in vitro and in vivo. Neuropharmacology 2015; 89: 168-174.
[37] Rahman MA, Jalouli M, Al-zharani M, Rahaman KA and Harrath AH. Interplay between hypoxia-inducible factors and apoptosis in glioblastoma. Biochem Pharmacol 2026; 244: 117619.
[38] Balamurugan K. HIF-1 at the crossroads of hypoxia, inflammation, and cancer. Int J Cancer 2016; 138: 1058-1066.
[39] Lee HR, Leslie F and Azarin SM. A facile in vitro platform to study cancer cell dormancy under hypoxic microenvironments using CoCl2. J Biol Eng 2018; 12: 12.
[40] Wang E, Zhang C, Polavaram N, Liu F, Wu G, Schroeder MA, Lau JS, Mukhopadhyay D, Jiang SW, O'Neill BP, Datta K and Li J. The role of factor inhibiting HIF (FIH-1) in inhibiting HIF-1 transcriptional activity in glioblastoma multiforme. PLoS One 2014; 9: e86102.
[41] Semenza GL. Hypoxia-inducible factors: mediators of cancer progression and targets for cancer therapy. Trends Pharmacol Sci 2012; 33: 207-214.
[42] Yun HJ, Li M, Guo D, Jeon SM, Park SH, Lim JS, Lee SB, Liu R, Du L, Kim SH, Shin TH, Eyun SI, Park YY, Lu Z and Lee JH. AMPK-HIF-1α signaling enhances glucose-derived de novo serine biosynthesis to promote glioblastoma growth. J Exp Clin Cancer Res 2023; 42: 340.
[43] Lopez-Fabuel I, Le Douce J, Logan A, James AM, Bonvento G, Murphy MP, Almeida A and Bolaños JP. Complex I assembly into supercomplexes determines differential mitochondrial ROS production in neurons and astrocytes. Proc Natl Acad Sci U S A 2016; 113: 13063-13068.
[44] Saldana-Caboverde A, Nissanka N, Garcia S, Lombès A and Diaz F. Hypoxia promotes mitochondrial complex I abundance via HIF-1α in complex III and complex IV eficient cells. Cells 2020; 9: 2197.
[45] Acín-Pérez R, Fernández-Silva P, Peleato ML, Pérez-Martos A and Enriquez JA. Respiratory active mitochondrial supercomplexes. Mol Cell 2008; 32: 529-539.
[46] Lobo-Jarne T and Ugalde C. Respiratory chain supercomplexes: structures, function and biogenesis. Semin Cell Dev Biol 2018; 76: 179-190.
[47] Signes A and Fernandez-Vizarra E. Assembly of mammalian oxidative phosphorylation complexes I-V and supercomplexes. Essays Biochem 2018; 62: 255-270.
[48] García-Poyatos C, Cogliati S, Calvo E, Hernansanz-Agustín P, Lagarrigue S, Magni R, Botos M, Langa X, Amati F, Vázquez J, Mercader N and Enríquez JA. Scaf1 promotes respiratory supercomplexes and metabolic efficiency in zebrafish. EMBO Rep 2020; 21: e50287.
[49] Kim JW, Tchernyshyov I, Semenza GL and Dang CV. HIF-1-mediated expression of pyruvate dehydrogenase kinase: a metabolic switch required for cellular adaptation to hypoxia. Cell Metab 2006; 3: 177-185.
[50] Maranzana E, Barbero G, Falasca AI, Lenaz G and Genova ML. Mitochondrial respiratory supercomplex association limits production of reactive oxygen species from complex I. Antioxid Redox Signal 2013; 19: 1469-1480.
[51] Griguer CE, Flor S and Oliva CR. From structure to vulnerability: mitochondrial supercomplexes in cancer cells. Cells 2026; 15: 258.
[52] Hollinshead KER, Parker SJ, Eapen VV, Encarnacion-Rosado J, Sohn A, Oncu T, Cammer M, Mancias JD and Kimmelman AC. Respiratory supercomplexes promote mitochondrial efficiency and growth in severely hypoxic pancreatic cancer. Cell Rep 2020; 33: 108231.
[53] Wu Q, Wu WS, Su L, Zheng X, Wu WY, Santambrogio P, Gou YJ, Hao Q, Wang PN, Li YR, Zhao BL, Nie G, Levi S and Chang YZ. Mitochondrial ferritin is a hypoxia-inducible factor 1α-inducible gene that protects from hypoxia-induced cell death in brain. Antioxid Redox Signal 2019; 30: 198-212.
[54] Quirós PM, Español Y, Acín-Pérez R, Rodríguez F, Bárcena C, Watanabe K, Calvo E, Loureiro M, Fernández-García MS, Fueyo A, Vázquez J, Enríquez JA and López-Otín C. ATP-dependent Lon protease controls tumor bioenergetics by reprogramming mitochondrial activity. Cell Rep 2014; 8: 542-556.
[55] Ghosh JC, Seo JH, Agarwal E, Wang Y, Kossenkov AV, Tang HY, Speicher DW and Altieri DC. Akt phosphorylation of mitochondrial Lonp1

protease enables oxidative metabolism and advanced tumor traits. Oncogene 2019; 38: 6926-6939.
[56] Cole A, Wang Z, Coyaud E, Voisin V, Gronda M, Jitkova Y, Mattson R, Hurren R, Babovic S, Maclean N, Restall I, Wang X, Jeyaraju DV, Sukhai MA, Prabha S, Bashir S, Ramakrishnan A, Leung E, Qia YH, Zhang N, Combes KR, Ketela T, Lin F, Houry WA, Aman A, Al-Awar R, Zheng W, Wienholds E, Xu CJ, Dick J, Wang JC, Moffat J, Minden MD, Eaves CJ, Bader GD, Hao Z, Kornblau SM, Raught B and Schimmer AD. Inhibition of the mitochondrial protease ClpP as a therapeutic strategy for human acute myeloid leukemia. Cancer Cell 2015; 27: 864-876.
[57] Seo JH, Rivadeneira DB, Caino MC, Chae YC, Speicher DW, Tang HY, Vaira V, Bosari S, Palleschi A, Rampini P, Kossenkov AV, Languino LR and Altieri DC. The mitochondrial unfoldase-peptidase complex ClpXP controls bioenergetics stress and metastasis. PLoS Biol 2016; 14: e1002507.
[58] Sathe S, Li Q, Jung J and Wu J. Targeting the mitochondria in high-grade gliomas. Cancers 2025; 17: 3062.
[59] Lee YG, Kim HW, Nam Y, Shin KJ, Lee YJ, Park DH, Rhee HW, Seo JK and Chae YC. LONP1 and ClpP cooperatively regulate mitochondrial proteostasis for cancer cell survival. Oncogenesis 2021; 10: 18.
[60] Guo R, Gu J, Wu M and Yang M. Amazing structure of respirasome: unveiling the secrets of cell respiration. Protein Cell 2016; 7: 854-865.
[61] Fernandez-Vizarra E, López-Calcerrada S, Tzoulis C, Pitceathly R, Zeviani M and Ugalde C. Two respiratory chain organizations with distinct bioenergetic properties coexist in human mitochondria. Biochim Biophys Acta Bioenerg 2022; 1863: 148698.
[62] Ikeda K, Horie-Inoue K, Suzuki T, Hobo R, Nakasato N, Takeda S and Inoue S. Mitochondrial supercomplex assembly promotes breast and endometrial tumorigenesis by metabolic alterations and enhanced hypoxia tolerance. Nat Commun 2019; 10: 4108.
[63] Williams EG, Wu Y, Jha P, Dubuis S, Blattmann P, Argmann CA, Houten SM, Amariuta T, Wolski W, Zamboni N, Aebersold R and Auwerx J. Systems proteomics of liver mitochondria function. Science 2016; 352: aad0189.
[64] Porras CA and Bai Y. Respiratory supercomplexes: plasticity and implications. Front Biosci (Landmark Ed) 2015; 20: 621-634.
[65] Pérez-Pérez R, Lobo-Jarne T, Milenkovic D, Mourier A, Bratic A, García-Bartolomé A, Fernández-Vizarra E, Cadenas S, Delmiro A, García-Consuegra I, Arenas J, Martín MA, Larsson NG and Ugalde C. COX7A2L is a mitochondrial complex III binding protein that stabilizes the III2+IV supercomplex without affecting respirasome formation. Cell Rep 2016; 16: 2387-2398.
[66] Mourier A, Matic S, Ruzzenente B, Larsson NG and Milenkovic D. The respiratory chain supercomplex organization is independent of COX7a2l isoforms. Cell Metab 2014; 20: 1069-1075.
[67] Vercellino I and Sazanov LA. Structure and assembly of the mammalian mitochondrial supercomplex CIII(2)CIV. Nature 2021; 598: 364-367.